This is an open access article published under an ACS AuthorChoice License, which permits copying and redistribution of the article or any adaptations for non-commercial purposes.

Journal of Medicinal Chemistry

Article

pubs.acs.org/jmc

Synthesis, Binding and Antiviral Properties of Potent Core-Extended Naphthalene Diimides Targeting the HIV-1 Long Terminal Repeat Promoter G-Quadruplexes

Rosalba Perrone,[†,§] Filippo Doria,[‡,§] Elena Butovskaya,[†,§] Ilaria Frasson,[†] Silvia Botti,[‡] Matteo Scalabrin,[†] Sara Lago,[†] Vincenzo Grande,[‡] Matteo Nadai,[†] Mauro Freccero,*[,‡] and Sara N. Richter*[,†]

[†]Department of Molecular Medicine, University of Padua, via Gabelli 63, 35121 Padua, Italy

[‡]Department of Chemistry, University of Pavia, V.le Taramelli 10, 27100 Pavia, Italy

Supporting Information

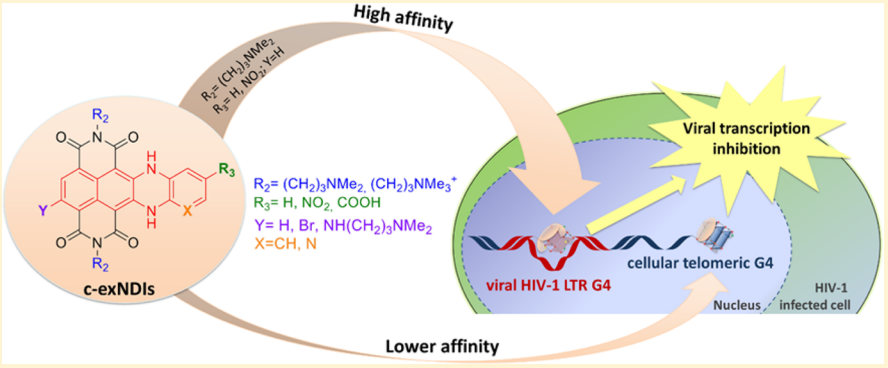

ABSTRACT: We have previously reported that stabilization of the G-quadruplex structures in the HIV-1 long terminal repeat (LTR) promoter suppresses viral transcription. Here we sought to develop new G-quadruplex ligands to be exploited as antiviral compounds by enhancing binding toward the viral G-quadruplex structures. We synthesized naphthalene diimide derivatives with a lateral expansion of the aromatic core. The new compounds were able to bind/stabilize the G-quadruplex to a high extent, and some of them displayed clear-cut selectivity toward the viral G-quadruplexes with respect to the human telomeric G-quadruplexes. This feature translated into low nanomolar anti-HIV-1 activity toward two viral strains and encouraging selectivity indexes. The selectivity depended on specific recognition of LTR loop residues; the mechanism of action was ascribed to inhibition of LTR promoter activity in cells. This is the first example of G-quadruplex ligands that show increased selectivity toward the viral G-quadruplexes and display remarkable antiviral activity.

INTRODUCTION

G-quadruplexes (G4s) are nucleic acids secondary structures that may form in single-stranded G-rich sequences under physiological conditions.[1−3] Four Gs bind via Hoogsteen-type hydrogen bonds base-pairing to yield G-quartets, which in turn stack on top of each other to form the G4. G4 structures may significantly vary, both in terms of strand stoichiometry (forming both inter- and intramolecular structures) and strand orientation/topology. The presence of K^+ cations specifically supports G4 formation and stability.[4−6] In the human genome and in prokaryotes, G4 DNA motifs have been found in telomeres, G-rich micro- and mini-satellites, near oncogene promoters, and within the rDNA.[7−12] Human G4 DNA motifs have been reported to be associated with recombination prone regions[13] and to show mutational patterns that preserve the potential to form G4 DNA structures.[9] Misregulation of these G4 structures has been associated with relevant human neurological disorders.[14−18] The identification of G4 binding proteins[19] and their visualization in cells with antibody-based technology[20,21] have also provided convincing evidence of the existence of cellular G4s in vivo.

Recently, the presence of G4s in viruses and their involvement in virus key steps has also been provided.[22] G4s have been implicated in pathogenic mechanisms of the Epstein−Barr virus[23,24] and the SARS coronavirus.[25] We and other groups have identified functionally significant G4s in the Nef coding region[26] and the unique long terminal repeat (LTR) promoter[27−29] of the human immunodeficiency virus (HIV), the etiologic agent of the acquired immune deficiency syndrome (AIDS). These studies have shown that G4 folding at the LTR promoter decreased viral transcription with an effect that was augmented by a G4 ligand.[27,30]

The involvement of G4 structures in several human diseases propelled the development of G4 ligands. Several aromatic cores with protonable side chains bind the G4 conformation,

Received: August 18, 2015
Published: November 24, 2015

 © 2015 American Chemical Society

DOI: 10.1021/acs.jmedchem.5b01283
J. Med. Chem. 2015, 58, 9639−9652

Scheme 1. Structure of BRACO-19 and Core-Extended NDIs (c-exNDIs) Reported in the Literature,[44,48−51] and the New Synthesized Water-Soluble c-exNDIs (lower right panel)

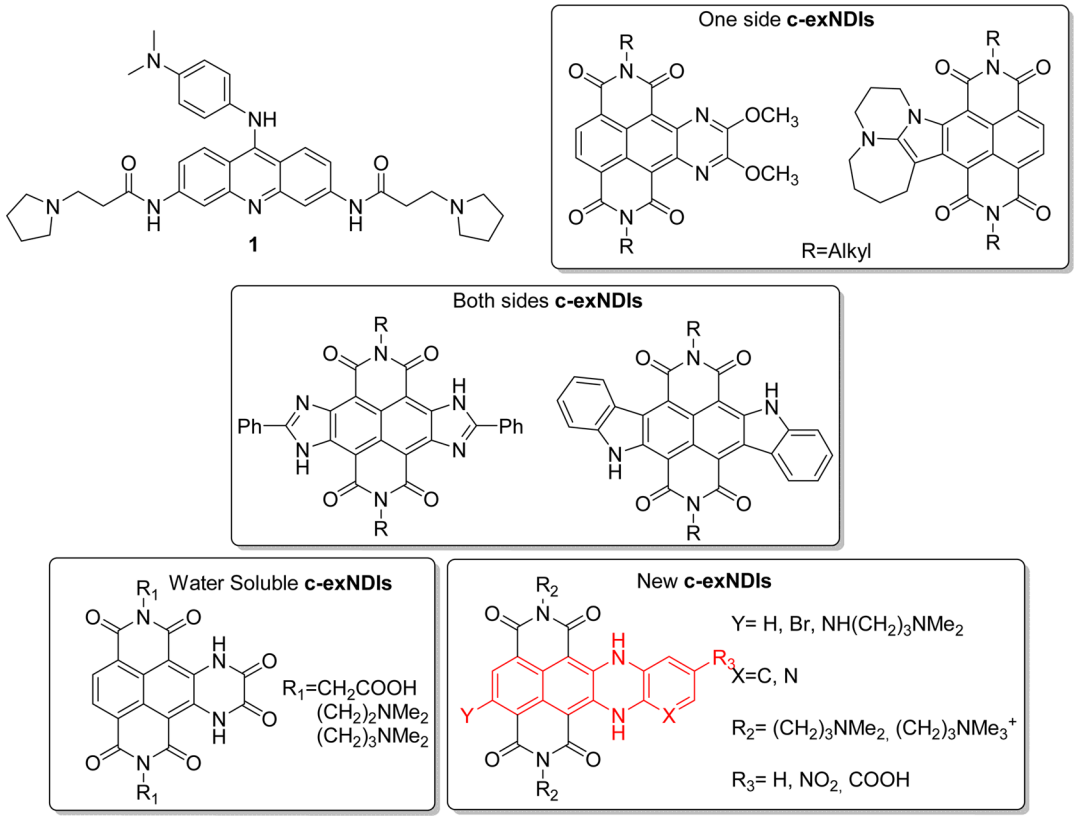

Scheme 2. Optimized Synthetic Protocol for the Preparation of Water-Soluble 2−11[a]

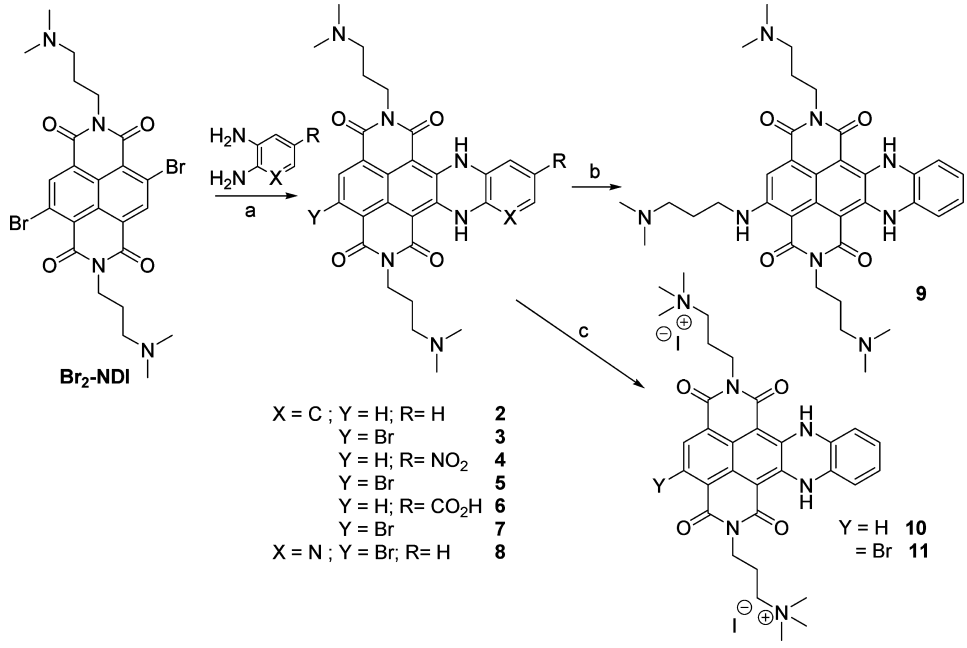

[a](a) DMF, 70°C, 16 h, under N_2; (b) *N*,*N*-dimethylpropylamine, MW, 150°C 3 min, closed vessel; (c) MeI, $CHCl_3$, rt, 16 h.

such as porphyrins,[31,32] acridines, such as **1** (BRACO-19, Scheme 1),[33,34] fluoroquinolones[35] anthraquinones, phenanthrolines, quinacridines, carbazoles, bis-indole carboxamides, triazoles, and benzimidazoles;[36] natural compound derivatives, such as berberine,[37] telomestatin,[38] quindolin,[39] several tetra-substituted perlyene tetracarboxylic' and water-soluble naphthalene diimide (NDIs).[41−46] So far, the vast majority of molecules has been tested against cellular G4s implicated in tumor pathogenesis: some compounds showed interesting antiproliferative properties;[36] in particular, quarfloxin pro-

DOI: 10.1021/acs.jmedchem.5b01283
J. Med. Chem. 2015, 58, 9639−9652

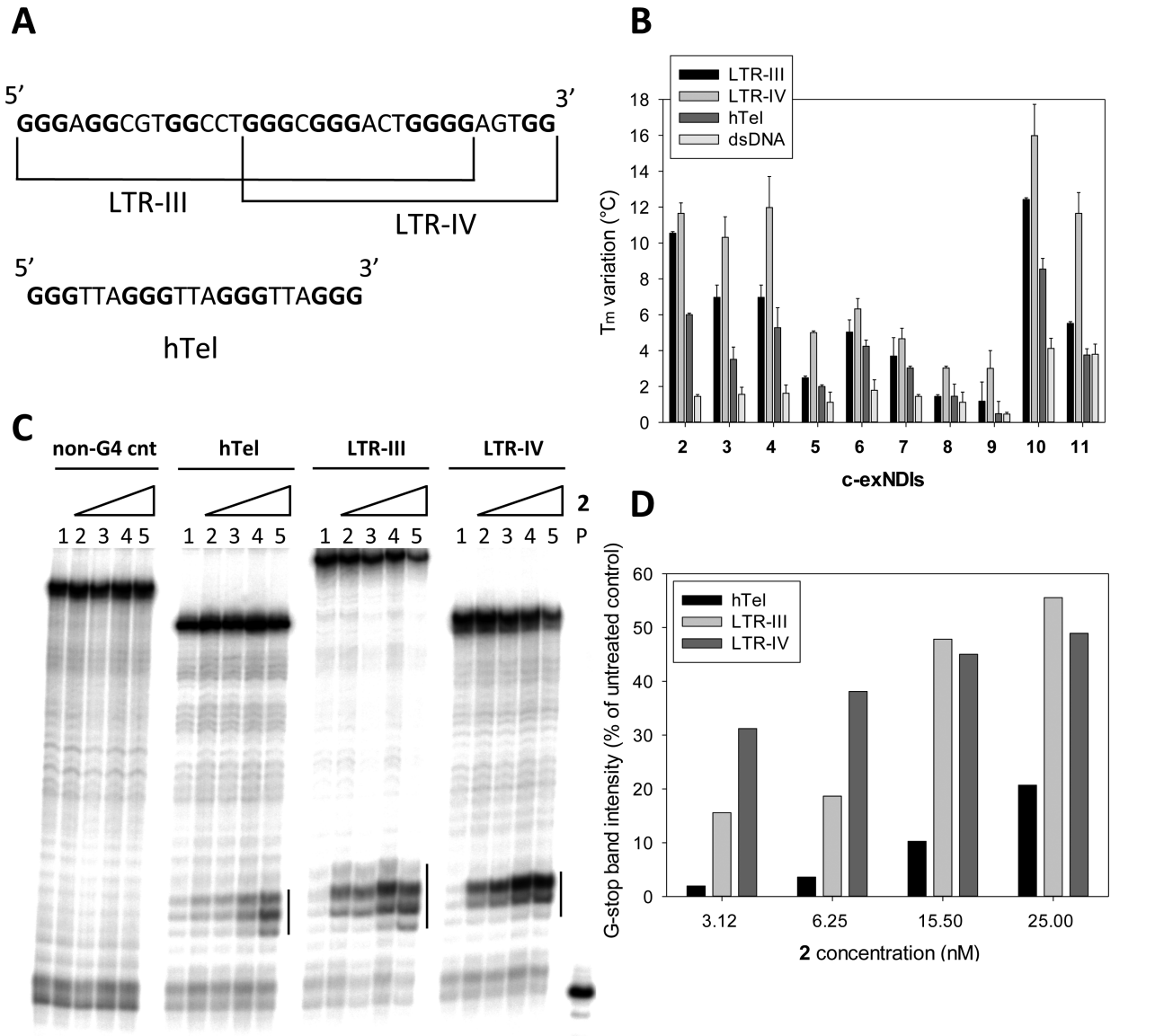

Figure 1. G4 stabilization by the **c-exNDIs**. (A) G4-forming sequences used in this study. (B) FRET analysis. ΔT_m values of HIV-1 LTR G4-folded sequences (LTR-III and LTR-IV), the G4-folded telomeric sequence (hTel), and a control double-stranded sequence (dsDNA) obtained upon addition of equimolar amounts of **2**–**11** (0.25 μM). (C) *Taq* polymerase stop assay. *Taq* polymerization was performed in the presence/absence of K^+ and **2**, as indicated, on the hTel, LTR-III, and LTR-IV templates, which were previously folded into G4. A control template unable to fold into G4 was also used (non-G4 cnt). Stop regions are highlighted by vertical bars. (D) Quantification of the intensity of the stop bands obtained in the *Taq* polymerase stop assay. Stop band intensity of the treated samples were normalized vs the untreated sample.

ceeded into phase II clinical trials, but its limited bioavailability prevented further progress.[35] Few molecules have been tested also as antiviral agents:[23,27,30,47] despite the low selectivity indexes, these studies have shown the possibility to develop antiviral molecules with a G-quadruplex-mediated mechanism of action.

The lateral expansion of the NDI core provided by our investigation may offer an additional opportunity to enhance both G4 binding potency and selectivity, discriminating G4 structures with different accessibility to the edge quartets. Examples that comprise the annulation of five- and six-membered heterocyclic rings either on one side of the NDI[48,49] or on both sides have been reported (Scheme 1).[50,51] Surprisingly, only one class of these core-extended NDIs (**c-exNDIs**) has been engineered water-soluble to be investigated as G4 ligand,[44] the others have found applications in the field of material chemistry and as pH sensors.[49−51]

Because of the possibility to block HIV-1 transcription by stabilizing the G4 structures present in the unique viral LTR promoter, we here synthesized and tested a series of novel **c-exNDIs** for both their binding to the LTR G4s and anti-HIV-1 activity. In these new structures, the NDI core has been merged to the dihydrobenzophenazine polynuclear heterocycle (highlighted in red in Scheme 1). We proved that these derivatives display binding and stabilization selectivity toward the viral G4s as compared to a telomeric G4 and that this translates into a therapeutic window where the compounds are active against the virus but not toxic for the cell.

DOI: 10.1021/acs.jmedchem.5b01283
J. Med. Chem. 2015, 58, 9639−9652

RESULTS

Design and Synthesis of c-exNDIs. We have designed and synthesized a small library of new and water-soluble **c-exNDIs** (**2**−**11**, Scheme 2), where the NDI core has been merged to the dihydrobenzophenazine polynuclear heterocycle (highlighted in red in Scheme 1). The choice has been made based on the pK_a values of the *N*,*N*-dimethylpropan-amine side chains: the pK_a values are above 7 (pK_{a1} = 8.1, pK_{a2} = 8.6),[52] suggesting that the side chains are mainly protonated under physiological conditions. This aspect ensures good solubilizing properties, reducing self-aggregations. We discharged the shorter *N*,*N*-dimethylthyl-amine side chains, as their pK_a values are much lower (pK_{a1} = 5.6, pK_{a2} = 7.4). The **c-exNDIs** are structurally characterized by a larger flat core than the NDIs. This feature should improve π-stacking interaction implementing the binding to the G4. Indeed, DFT calculation performed at B3LYP/6-31+G(d,p) level of theory in gas phase indicated that the dimension of the **c-exNDI** core supported a more extensive overlap to the quartet of the G4 structure (Supporting Information, Figure S1). Enhancement of the ligand steric hindrance accessing the outside G4 quartets might offer an opportunity to implement selectivity as well. Furthermore, the proposed structural extension on the NDI scaffold should merge the useful optoelectronic properties (absorption, emission, and singlet oxygen sensitizer) of functionalized NDIs to those of substituted dihydrobenzophenazines. Compounds with both H and Br substituents at the Y position were considered to evaluate the effect of a bulky substituent (Br) at this position. To synthesize the **c-exNDIs**, we developed the synthetic protocol highlighted in Scheme 2. According to published methods, the imidation reaction of the readily available 2,6-dibromo-1,4,5,8-naphthalenetetracarboxylic dianhydride yielded the 2,6-dibromo-substituted NDI, under acidic conditions, in almost quantitative yield. Subsequently, a two-step protocol starting from a nucleophilic aromatic substitution (S_NAr) in the presence of an excess (2.5 equiv) of *ortho*-diaminophenyl derivatives in DMF as solvent at 70 °C for 16 h afforded a 60:40 mixture of monobrominated and debrominated products in an overall quantitative yield. The ring closing reaction following the S_NAr in one pot (step a, in Scheme 2) occurred through a Tchitchibabin mechanism, with the elimination of hydride favored by the formation of a six-membered ring. The second S_NAr on the remaining aromatic bromide was carried out by dissolving **3** in neat N^1,N^1-dimethylpropane-1,3-diamine. To improve the reaction yield, we optimized a microwave-assisted protocol (150 °C, 200 psi, 250 bar, 200 W, 3 min, sealed reaction vessels) to give product **9**, which crystallized from the reaction mixture. We achieved the synthesis of the permanently charged quaternary ammonium salts **10** and **11** with a classical exhaustive methylation, in the presence of MeI at rt for 16 h. All the synthesized ligands (**2**−**11**) were purified by preparative HPLC (CH_3CN:H_2O and 0.1% CF_3COOH as eluent). Further anion exchange yielded **2**−**9** as hydrochloride salts. On the contrary, **10** and **11** were investigated as iodide quaternary ammonium salts.

c-exNDIs Greatly Stabilize G4 with a Preference for the LTR Conformations vs the Telomeric Sequence. To detect the ability of the new **c-exNDIs** to bind and stabilize the G4 conformations of the HIV-1 LTR promoter, two G4-forming LTR sequences were employed: LTR-III and LTR-IV, both composed of four GGG tracts (Figure 1A). When embedded within the full-length G-rich sequence of the LTR promoter, LTR-III is the most stable G4, while LTR-IV folds when induced by G4 ligands.[27] A FRET melting assay was performed to assess the degree of stabilization of the LTR-III and LTR-IV G4 by **c-exNDIs**. The minimal intramolecular G4-forming human telomeric (hTel) sequence (Figure 1A) was employed to evaluate the activity of the **c-exNDIs** on one of the most highly represented and accessible cellular G4: in fact, the TTAGGG repeat is present as 2000−3000 double-stranded (ds) and 50−200 single-stranded sequences at the human telomeres.[53] A double-stranded (ds) DNA was also added to address specificity toward the G4 conformation (Supporting Information, Table S1). While this kind of assay is typically performed using molar excess of the tested compounds, we here initially employed equimolar amounts of the target DNA sequence and compounds (i.e., 0.25 μM) to better differentiate the stabilization efficiency among the different **c-exNDIs**. The melting temperatures of the LTR-III, LTR-IV, hTel, and dsDNA G4 conformations were sufficiently similar (66.9, 61.9, 66.9, and 66.5 °C, respectively) to allow a meaningful comparison. In the presence of the **c-exNDIs**, a marked increase in the stabilization of the G4-forming oligonucleotides was observed (Figure 1B and Supporting Information, Table S2). Among the tested **c-exNDIs**, **2**, **3**, **4**, **10**, and **11** were the most efficient ligands, with a stabilization on LTR-IV G4 of 10−16 °C at equimolar amounts. At 4-fold **c-exNDI**:DNA molar ratio, the stabilization increased to above 25 °C, which is the maximum increase measurable in these settings (data not shown). The other **c-exNDIs** showed intermediate (4 °C ≤ ΔT_m < 7 °C, **5**, **6**, and **7**), or low (ΔT_m < 4 °C, **8** and **9**) level of stabilization on LTR-IV G4. Compounds **2** and **10** stabilized LTR-III G4 above 10 °C. Among the G4 structures, hTel G4 was the least efficiently stabilized, whereas stabilization on dsDNA was negligible. Only compounds **10** and **11** displayed a significant stabilization on dsDNA, indicating that the presence of two permanent charges (the quaternary ammonium moieties) favors an unspecific binding to the negatively charged nucleic acid. In general, the H series of all derivatives (Y = H, **2**, **4**, **6**, **10**; Scheme 2) was more active and more selective for the viral G4s compared to the Br substituted ones (Y = Br, **3**, **5**, **7**, **8**; Scheme 2). Compounds **2**, **3**, and **10** exhibited a difference in stabilization of LTR-IV G4s vs hTel G4 equal or above 6 °C, which roughly corresponds to 40% of the overall stabilization efficiency (Figure 1B and Supporting Information, Table S2).

Because oligonucleotides used for FRET analysis display fluorophore-modified ends that may influence the measured stabilization, additional techniques using label-free oligonucleotides were employed. Compound **2**, a representative of the best ligands, was assayed by circular dichroism (CD) on LTR-IV, LTR-III, and hTel G4s. At 4:1 **c-exNDI**:DNA ratio, a stabilization higher than 27 °C was obtained on both LTR-III and LTR-IV (Supporting Information, Figures S2A and S2B), while hTel G4s was stabilized by only 19.9 °C (Supporting Information, Figure S2C), confirming a preference for the viral G4s. A *Taq* polymerase stop assay was performed on the LTR-III, LTR-IV, and hTel templates. A control template unable to fold into G4 was used to exclude unspecific inhibition of the polymerase enzyme by the **c-exNDI**. Compound **2** induced an intense stop site at the most 3′ G tract in each G4-forming template (Figure 1C), indicating effective stabilization of the G4 conformation by the compound. This effect was significantly more relevant on the viral sequences vs the

DOI: 10.1021/acs.jmedchem.5b01283
J. Med. Chem. 2015, 58, 9639−9652

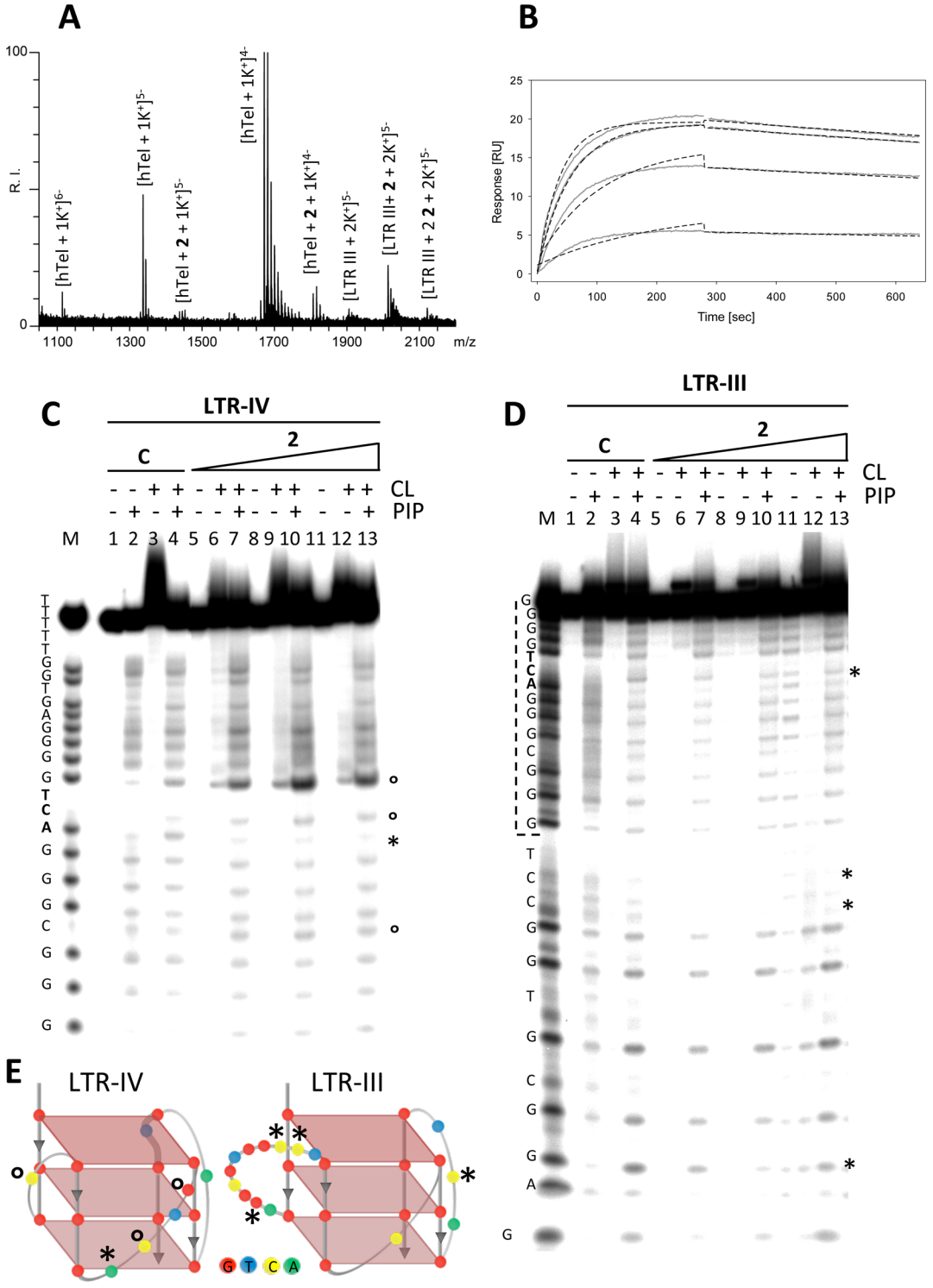

Figure 2. Affinity and binding site analysis. (A) ESI/MS competition assay. Representative spectrum. Equimolar amounts of LTR-III and hTel were incubated with 2-fold excess of **2** and analyzed by ESI/MS. The identity of *m*/*z* signals is shown above each signal. RI stands for relative intensity. (B) SPR analysis of **2** binding toward the LTRs and hTel G4s. Representative sensorgram of **2** binding to LTR-III G4. Biosensor data were collected at 25 °C; the compound was injected at increasing concentrations (26, 40, 59, 89, 133, 200 nM). Sensorgrams are shown as gray lines. Dotted black lines represent local 1:1 binding fits obtained for a calculated R_{max}. (C,D) CL-mediated footprinting. LTR-IV (C) and LTR-III (D) oligonucleotides were G4 folded, incubated with increasing amounts of **2** (lanes 5−13), alkylated with CL (CL lanes), and subjected to hot piperidine treatment (PIP lanes) to induce cleavage of the phosphodiester bond at the alkylated bases. (C) Lanes 1−4 are control lanes not treated with the **c-exNDI**. The symbols * and ○ indicate base protection and exposure, respectively. M is a marker lane obtained by the Maxam and Gilbert sequencing of the oligonucleotides. The oligonucleotide sequence is shown on the left. The vertical dotted bar indicates the region of the LTR-III shared with LTR-IV. (E) Schematics of the LTR-IV and LTR-III G4 conformations. The represented LTR-IV G4 topology has been solved by NMR (PDB code 2N4Y); the shown LTR-III G4 conformation derives from previous low resolution structural data.[27]

DOI: 10.1021/acs.jmedchem.5b01283
J. Med. Chem. 2015, 58, 9639−9652

Table 1. Relative Binding Affinity of 2 and 4 for the LTR-III, LTR-IV, hTel, c-kit2 (kit), and c-myc (myc) G4-Folded Oligonucleotides

	binding affinity[68]					
	c-exNDI 2			c-exNDI 4		
competing G4s	LTR-III	LTR-IV	cell G4 (hTel, kit, or myc)	LTR-III	LTR-IV	cell G4 (hTel, kit, or myc)
LTR-III/hTel	80		10	82		10
LTR-IV/hTel		52	25		75	18
LTR-III/LTR-IV	71	25		80	68	
LTR-III/kit	33		12	54		18
LTR-IV/kit		25	9		55	23
LTR-III/myc	39		45	51		37
LTR-IV/myc		25	44		71	45

telomeric template (Figure 1D), confirming again a preferential stabilization of the viral G4s.

The above techniques evaluated stabilization of the G4 conformation as an indicator of the efficiency of the interaction of the ligands with the tested G4 structures. Binding affinity was next directly assessed by two different methods.

Competition electrospray ionization mass spectrometry (ESI-MS) experiments[54−56] allowed establishment of the relative affinity of the **c-exNDIs** toward the G4 sequences. We first confirmed by CD analysis that in the buffer conditions used for the ESI/MS experiments the topology of the G4-folded oligonucleotides did not significantly modify (Supporting Information, Figure S3) Equimolar amounts of LTR-III/hTel, LTR-IV/hTel, and LTR-III/LTR-IV G4s were incubated with 2-fold molar excess of compounds **2** or **4**. Because ESI/MS transfers intact biomolecules complexes in the gas phase and signal intensity is proportional to the abundance of each species in solution, the ratio between m/z signals of each bound species and the corresponding bound and free G4 (Figure 2A) was calculated (Table 1). While LTR-III and LTR-IV were detected mostly as all-bound species, hTel was mostly unbound (Figure 2A, and Supporting Information, Figures S4A and S4B). This analysis clearly shows that our **c-exNDIs** preferentially bind the two viral sequences over the telomeric sequence. To corroborate the selectivity toward the viral sequences, two additional cellular G4 folding sequences were evaluated: c-kit2[57] and c-myc.[32] The LTR G4s were preferred over c-kit2 G4 by both compounds; in the case of c-myc G4, compound **4** preferentially bound to the LTR G4s, whereas compound **2** showed more intense binding to c-myc (Table 1). Therefore, we confirmed a general, even though not absolute, selectivity toward the LTR G4s. It is also possible that the much higher stability of the c-myc G4 (T_m > 95 °C) vs the stability of the other tested G4s (LTR-III 66.9 °C, LTR-IV 61.9 °C, c-kit2 72.1 °C) played a role in this result. When the two LTR G4s were competed with each other, the LTR-III sequence was preferred. At 2-fold excess of compound, LTR-III bound up to two molecules of compounds, whereas only one molecule was obtained for both LTR-IV and hTel (Figure 2, and Supporting Information, Figure S5). At saturating concentrations (10-fold molar excess), three molecules were bound to LTR-III G4, whereas up to two molecules could bind LTR-IV and hTel G4s (Supporting Information, Figure S5).

Next, absolute affinity of **2** was measured by surface plasmon resonance (SPR) toward the three G4-folded sequences. This analysis confirmed that LTR-III G4 displays the highest binding affinity (K_D 3.2 nM), followed by LTR-IV G4 (K_D 6.1 nM); hTel G4 exhibited the lowest affinity (K_D 13.1 nM) (Figure 2B, and Supporting Information, Figure S6). The binding affinity of the Br derivatives with each of the substituents in position R against LTR-IV was next assessed. Compounds **3** and **5** had K_D values similar to that of **2** (K_D 6.6 and 5.9 nM, respectively), **10** displayed an increased binding affinity (K_D 1.7 nM), whereas **7** and **11** showed the lowest affinity (K_D 21.6 and 12.9 nM, respectively). These data are in line with the stabilization properties observed for these derivatives by FRET and CD analysis and confirm the improved and reduced recognition properties of the **c-exNDIs** exhibiting permanent dicationic (**10**) and neutral or monocationic charge states (**7**), respectively, under physiological conditions. They also confirm that a bulky substituent in position Y of the NDI core (**11**, Scheme 2) highly reduces binding, whereas a NO_2 group in position R maintains excellent binding properties (**5**, Scheme 2).

We reasoned that the observed biased affinity for the LTR sequences could derive by specific binding of the **c-exNDIs** to structural/sequence features shared by the LTR G4s. To this end, we evaluated the protection exerted by compound **2** over residues of the LTR G4s against clerocidin (CL). This molecule has been shown to alkylate DNA single-stranded G, C, and A bases[58,59] and to be able to predict G4 structural folding.[60] Labeled oligonucleotides were folded, treated with increasing amounts of **2**, exposed to CL, and further treated with piperidine to highlight CL-alkylated sites. In these settings, we expected to visualize only loop bases bound by the **c-exNDI** because base-paired Gs involved in G-quartet formation would not be available to CL alkylation, independently of the presence of the compound. The NMR structure of LTR-IV has been solved (PDB code 2N4Y), and therefore we were able to assess that nucleotides affected by the presence of the **c-exNDI** were in two loops of the structure: in particular, in the ACTG loop the A base was protected, whereas C and G were exposed; in the 1-base-loop, the C base was exposed (Figure 2C and 2E). The structure of LTR-III has not been solved yet, however, previous data indicated that this G4 can fold into different conformations, the main one of which is likely the one depicted in Figure 2E, as detected by low-resolution structural data.[27] In this case, we observed protection of the C base in the ACTG loop (Figure 2D), which is shared with the LTR-IV sequence (see Figure 1A); three additional residues (C, C, and G) were protected in the 11-base-loop (Figure 2D and 2E). Protection and exposure of residues indicated specific interaction of **2** at the affected LTR sites. Interestingly, unique LTR loops and in particular the ACTG loop shared by both LTR-III and LTR-IV, and absent in the telomeric sequence, were involved, indicating that these are likely the moieties that induce selectivity. We cannot exclude that other regions are bound by the **c-exNDI**, but probably the interaction at other sites is less stable or more

DOI: 10.1021/acs.jmedchem.5b01283
J. Med. Chem. 2015, 58, 9639−9652

Table 2. Antiviral Effects of the c-exNDI Derivatives and the Control 1 against Two HIV-1 Strains in TZM-bl Cells[a]

	IC_{50} (nM)			SI		TW (nM)	
c-exNDI	HIV-1 strain NL4-3	HIV-1 strain BaL	CC_{50} (nM)	HIV-1 strain NL4-3	HIV-1 strain BaL	HIV-1 strain NL4-3	HIV-1 strain BaL
2	13.2 ± 0.1	36.2 ± 4.3	532.0 ± 11.7	40	14	3.9−250.0	15.6−250.0
3	15.7 ± 2.1	32.5 ± 7.1	343.2 ± 32.2	22	11	7.8−125.0	15.6−125.0
4	11.0 ± 0.3	nd	188.0 ± 4.08	17	nd	3.9−125.0	nd
5	23.0 ± 1.3	nd	439.0 ± 10.7	19	nd	15.6−250.0	nd
6	975.3 ± 16.2	nd	> 5000	>5	nd	800−5000	nd
7	862.6 ± 31.5	nd	> 5000	>6	nd	800−5000	nd
8	63.5 ± 4.8	nd	458.1 ± 54.0	7.2	nd	no TW	nd
9	814.3 ± 36.4	nd	1759.9 ± 62.5	2.2	nd	no TW	nd
10	>5000	nd	>5000		nd	no TW	nd
11	> 000	nd	>5000		nd	no TW	nd
1	3400 ± 140[b]	nd	>12000[b]	>3.5	nd	3000−12000	nd

[a]NL4−3 and BaL are X4 and R5, respectively, HIV-1 strains. IC_{50} is the compound concentration required to inhibit 50% of HIV-1 production; CC_{50} is the compound concentration at which 50% of cell toxicity is observed; SI is the selectivity index; TW is the therapeutic window concentration. nd stands for "not determined". [b]indicates values previously reported.[27]

dynamic so that a clear protection/exposure could not be observed.

The Extended Core NDIs Display Anti-HIV-1 Activity at Nanomolar Concentrations. We have previously shown that the HIV-1 viral promoter folds into dynamic G4s and that stabilization of these G4 conformations by the G4 ligand **1** represses viral transcription and virus production in infected cells with IC_{50} (the concentration required to inhibit 50% of virus production) in the low μM range.[27,30] The average selectivity index (SI) for **1** was 12. Given the **c-exNDI** binding/stabilization selectivity observed in vitro for the viral G4s vs the cellular G4, we set out to investigate the anti-HIV-1 activity of the newly synthesized **c-exNDI** derivatives. Compound entry was preliminarily measured by phase contrast and fluorescence microscopy, taking advantage of the blue-colored **c-exNDI** dyes (λ_{abs} = 555 and 600 nm, for the unsubstituted **2**) and their red fluorescence emission (λ_{em} = 610 and 655 nm, for **2**). After 30 min of incubation, compounds concentrated into the cell (Supporting Information, Figure S7). We next treated infected cells with increasing amounts of compounds and measured virus production; concurrently, the cytotoxic concentration (CC_{50}) of the **c-exNDIs** in the same conditions but on uninfected cells was measured by MTT assay. All compounds were tested against the HIV-1 NL4-3 strain, which is a X4 strain. Results are reported in Table 2. Compounds **2**, **3**, **4**, and **5** displayed inhibitory concentration (IC_{50}) values below 25 nM. Compound **2** displayed a promising SI of 40, the best among the tested **c-exNDIs**, whereas SI values of compound **3**, **4**, and **5** were around 20, again superior to **1**. Derivatives **6** and **7** exhibited low activity and low cytotoxicity, while **9** showed the worst combination with low activity, high cytotoxicity, and SI of 2.2. We also evaluated the range of concentration (therapeutic window or TW), at which we obtained antiviral activity paralleled by less than 80% cytotoxicity. As shown in Figure 3A, **2** displayed the widest TW (3.9−250 nM); **4** and **5** also showed interesting TW values; TW concentrations for **6** and **7**, which are likely to be mainly monoanionic under physiological conditions as both the $(CH_2)_3NHMe_2^+$ moieties exhibit a pK_a >8.1,[52] were in the μM range; no TW was observed for **8** and **9** (Table 1). Finally, **10** and **11**, containing two quaternary ammonium moieties, did not display any antiviral or cytotoxic activity likely due to their inability to enter the cells, as already shown for NDIs with permanent positive charges.[61] Compound **2** and **3** were also tested on the HIV-1 BaL strain, a R5 strain with a different tropism. In this case, IC_{50} values below 40 nM were obtained, with SI of 14 for the H derivative (Table 1). Note that the H series of all derivatives was more active than the Br substituted one. Moreover, all compounds displayed CC_{50} values higher than 2 μM against a human fibroblast cell line.

The NDIs Derivatives Inhibit HIV-1 LTR Promoter Activity. It has been reported that compounds with multiple positive charges can block viral entry by interfering with the CXCR4 coreceptor.[62] To rule out this unspecific mechanism of action of the **c-exNDI**, we treated TZM-bl cells at 0, 1, and 2 h post infection (pi) with compound **2** and tested virus production at 31 h pi. No significant difference in the activity of the compound was observed at the tested times (Figure 3B). Zidovudine (AZT), a reference drug that targets the reverse transcriptase step,[63] displayed a behavior similar to that of the **c-exNDI**, maintaining activity from 0 to 2 h pi. In contrast, dextran sulfate (DS), a reference entry inhibitor,[64] exhibited antiviral effect only when added at 0 h pi. (Figure 3B). These data indicate that the initial steps are not targeted by **2**, which is thus active at/after 2 h pi, i.e., after the entry process has occurred.

We next tested the ability of **2** to reduce the activity of the HIV-1 LTR promoter in an EGFP reporter assay in HeLa-tat-III cells, which is a cell line stably transfected with a plasmid embedding the EGFP coding region under the control of the HIV-1 LTR promoter. Cells were treated with increasing concentrations of the **c-exNDI**, and the intensity of EGFP fluorescence was assessed by FACS analysis. A steady decrease in the mean levels of EGFP was observed at noncytotoxic concentrations of **2** (up to 60% of inhibition) (Figure 3C). To check if the activity of the **c-exNDI** at the LTR promoter was specific for the G4 conformation, two point mutations that abolish G4 folding were introduced in the LTR sequence (M4 + 5 LTR).[27] The wt LTR and M4 + 5 LTR luciferase reporter plasmids were transiently transfected into 293T cells either alone or in the presence of increasing amounts of compound **2**, and the luciferase signal was measured. Again, an important inhibition of LTR activity was observed on the wt LTR (up to 65% inhibition), whereas no effect was detected on the non-G4-forming mutant LTR sequence (Figure 3D). These data indicate a G4-mediated inhibition of the viral promoter by the **c-exNDI**.

DOI: 10.1021/acs.jmedchem.5b01283
J. Med. Chem. 2015, 58, 9639−9652

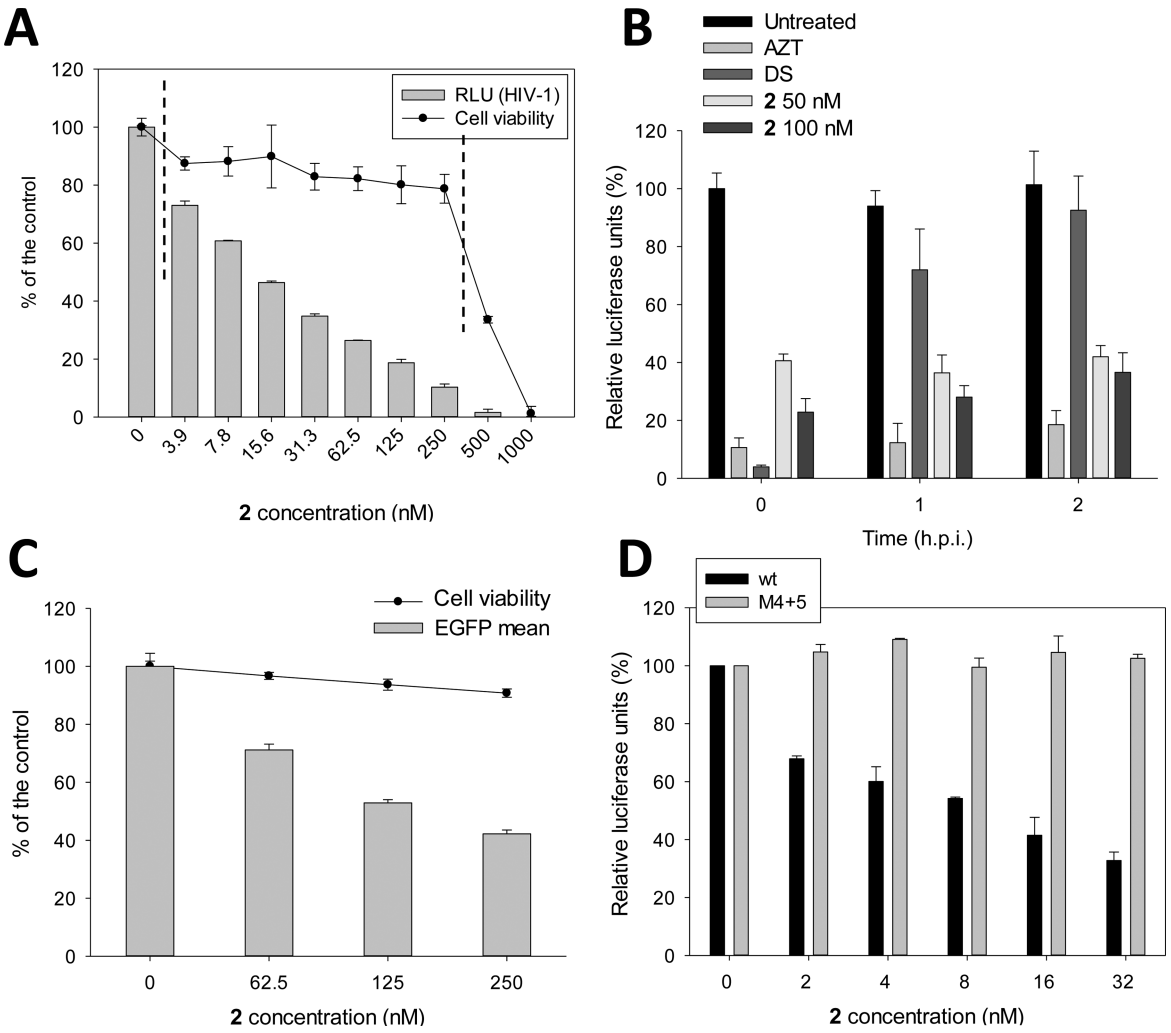

Figure 3. Antiviral activity of **c-exNDIs** and mechanism of action. (A) TZM-bl cells were infected with HIV-1 NL4-3 strain and treated with increasing concentrations (3.9−1000 nM) of the **c-exNDIs**. Uninfected cells were treated in the same conditions. Antiviral activity, expressed as relative luciferase units (RLU), was measured on infected cells, while cell viability was in parallel obtained with a MTT assay on the uninfected cells. The vertical dotted lines define the therapeutic window (TW) where the compound is active against the virus and not toxic against the cells. This figure is representative of the antiviral/cytotoxicity/TW experiments performed with the whole series of **c-exNDI** compounds. (B) Entry assay. TZM-bl cells were treated with the compound **2** (50−100 nM), AZT (0.5 μg/mL), or the entry inhibitor DS (100 μg/mL) at 0, 1, or 2 h pi. Virus production was measured at 31 h pi as RLU. The control depicts cells infected with the virus lacking compound treatment. (C) Effect of **2** on the LTR promoter activity compared to cytotoxicity. HeLa cells with a stably transfected LTR-EGFP reporter plasmid were treated with increasing concentrations of **2** (62.5−250 nM). EGFP mean was measured by FACS analysis. Cytotoxicity was estimate in parallel by gating on forward scatter (FSC) vs side scatter (SSC) using untreated cells as reference. (D) Specificity of the **2**-induced inhibition of LTR promoter activity on the G4 LTR conformation. 293T cells were transiently transfected with plasmids with the wt or M4 + 5 mutant LTR promoter sequence upstream a luciferase reporter gene. Luciferase signals were measured as a function of increasing **2** amounts and normalized to total protein content.

DISCUSSION AND CONCLUSIONS

We have here shown the synthesis, G4 binding properties, and antiviral activity of a new series of NDI derivatives with an extended aromatic core. First, most of the new compounds displayed improved stabilization on G4 structures, with substantial increments in T_m above values previously reported for NDI derivatives.[41−46] This feature is an indication that the expansion of the aromatic surface allows a more effective recognition of the G4 structure. This may be due to a more extensive overlap to the quartet of the G4 structure, as inferred by the dimension of the **c-exNDI** core, evaluated by DFT calculation (Supporting Information, Figure S1). Second, these compounds exhibited a very promising antiviral activity. Compared to **1**,[30] the best antiviral **2**−**5** showed improved IC_{50} values (in the low nM vs low μM range). This feature may derive from the selectivity observed in vitro for the LTR G4s over the telomeric G4 structures. The viral and telomeric G4s are likely the two most abundant DNA G4 species in the cell during infection, therefore a preferential effect on the viral G4s would result in higher antiviral activity and lower cytotoxicity, as observed. The **c-exNDIs** displayed both selective binding affinity and stabilization for the viral G4s. Between the two LTR G4s, the LTR-III sequence was most efficiently bound by **2**, as measured by ESI/MS and SPR. Even though LTR-III (38 nts) and LTR-IV (29 nts) display an identical number of G-quartets, LTR-III offers longer loops that may accommodate additional molecules and therefore may display increased binding affinity. Indeed, at saturating concentrations, binding of up to three **c-exNDI** molecules was observed by ESI/MS with LTR-III compared to two molecules for LTR-IV. In

DOI: 10.1021/acs.jmedchem.5b01283
J. Med. Chem. 2015, 58, 9639−9652

addition, two loops in both LTR-III and LTR-IV G4s were shown to be involved in **c-exNDI** interaction by footprinting analyses. We suggest that the compounds interact with the edge G-quartets through the core NDI planar aromatic surface, while the extended moiety and side chains interact with the side loops, affording selectivity toward the LTR G4s. To our knowledge, this is the first example of this type of selectivity based on chemical recognition of specific residues; in fact, previously reported selectivity rather relied on the recognition of a G4 conformation.[65]

Analysis of the binding activity of the series of **c-exNDIs** led us to the following structure−activity relationship (SAR) conclusions: (i) the nonextended side of the **c-exNDI** core [position Y (Scheme 1)], lacking substituents as the introduction of an aminoalkyl side chain, highly hinders stabilization of the G4 structures (i.e., **9**); (ii) Br is allowed as Y substituent, but it lowers binding and selectivity toward the viral sequences. The Br group may both hinder specific interactions (hence lower selectivity) and partially distort the aromatic core from planarity (hence lower G4 binding); (iii) the pyridine ring in place of the benzene in the extended core is strongly detrimental (compound **8**). The fair antiviral activity is paralleled by moderate cytotoxicity, allowing no TW, possibly due to off-target activity; (iv) the NO_2 moiety is allowed (compounds **4** and **5**) as compound **4** is the most powerful and selective ligand toward LTR-III; (v) the negatively charged carboxylate group decrease the electrostatic component of the binding to the DNA G4s (compounds **6** and **7**); (vi) on the contrary, the permanently positively charged ammonium groups extensively increase binding to the target G4s by adding electrostatic interaction (compounds **10** and **11**). However, compounds with permanent charges are not suitable for cell entry and hence cannot be exploited for antiviral purposes. A scheme of the chemical properties that lead to high-affinity recognition and selectivity of the **c-exNDI** binders is reported in the graphical abstract.

In conclusion, we have reported a new class of G4 ligands able to discriminate G4 structures based on the chemical recognition of structural features that are unique to the selected G4 sequences. On one hand this approach opens the possibility to develop anti-HIV compounds with a new mechanism of action that may complement current clinical AIDS therapies; on the other hand, our work clearly highlights the possibility to selectively recognize G4 structures with small molecules, prompting the search and development of G4 ligands specific for G4s implicated in several important human diseases.

EXPERIMENTAL SECTION

Materials and General Procedures. Reagents, oligonucleotides, solvents, and chemicals were purchased from Alfa Aesar or Sigma-Aldrich and were used as supplied without further purification. TLC analysis was carried out on silica gel (Merck 60F-254) with visualization at 254 and 366 nm. HPLC analysis and purifications were performed using two different HPLC: Waters system combining a Delta 600 PUMP, a 2489 UV/vis detector and Fraction Collector III (for preparative and analytical), and an Agilent system series 1260 (for analytical). The analytical column was XSelect CSH Phenyl-Hexyl (150 mm × 4.6 mm) (Waters). The preparative column was XSelect CSH Prep phenyl−hexyl 5 μm (150 mm × 30 mm) (Waters). Flows were 1 or 1.4 mL/min for analytical and 27 mL/min for preparative. For the analytical analysis were used the following method A: (aqueous solvent: 0.1% trifluoroacetic acid in water; organic solvent, acetonitrile); method A = 1 mL/min, isocratic flow over 2 min 95% of aqueous solvent; gradient, 95% aqueous, gradually to 40% aqueous over 12 min and at the end an isocratic flow over 4 min. For the preparative purification was used the following method B: (aqueous solvent: 0.1% trifluoroacetic acid in water; organic solvent, acetonitrile); Method B = 27 mL/min, isocratic flow over 4 min 95% of aqueous solvent; gradient, 95% aqueous, gradually to 70% aqueous over 16 min and at the end an isocratic flow over 4 min). ^{1}H , ^{13}C NMR spectra were recorded on a Bruker ADVANCE 300 MHz spectrometer. The potentiometric titrations were made with a Radiometer TitraLab 90 titration system. UV/vis spectra were run on a Varian Cary 100 SCAN spectrophotometer with quartz cuvettes of the appropriate path length (0.1−1 cm) at 25.0 ± 0.1 °C. Emission spectra were recorded on a PerkinElmer LS 50B instrument.

Chemistry. General Methods. *Synthesis of Intermediates and Final Ligands.* Br_2NDI has been synthesized according to the published procedure.[52] The new ligands (**2**−**11**) were analyzed by HPLC (see Supporting Information, HPLC Purity Data), confirming ≥97.6% purity.

*Nucleophilic Aromatic Substitution/Tchichibabin Reaction: Synthesis of **2**−**5**, **8**.* The starting NDI (0.5 mmol) was dissolved into 20 mL of DMF in a round-bottom flask together with 1.0 mmol of *o*-phenyl-diamine derivatives, the mixture was stirred at 45 °C for 16 h under argon. The resulting dark-violet solution was basified with sodium bicarbonate aqueous solution and extracted with three portion of $CHCl_3$ (50 mL). The organic layers were collected, dried on $NaSO_4$, and evaporated under vacuo. The crude product was analyzed and purified by HPLC chromatography (CH_3CN:H_2O 0.1%TFA) according to analytical method A and preparative method B. HCl 1 M solution was added to each chromatographic portion. Solvent evaporation under vacuum afforded the product as hydrochloride salt.

***2**·2HCl.* Yield = 25.2%; dark-violet solid; mp dec >200 °C. ^{1}H NMR (300 MHz, CD_3OD): 7.74 (s, 2H), 7.11 (dd, *J* = 3.3, 5.7 Hz, 2H), 6.89 (dd, *J* = 3.3, 5.7 Hz, 2H), 4.06 (m, 4H); 3.26 (m, 4H), 2.94 (s, 12H), 2.14 (m, 4H). ^{13}C NMR (75 MHz, CD_3OD): 166.4, 164.3, 143.2, 128.7, 128.0, 127.0, 125.9, 123.0, 118.2, 96.0, 57.0, 56.0, 43.9, 38.5, 38.2, 24.9, 24.2. Anal. Calcd for $C_{30}H_{34}Cl_2N_6O_4$: C, 58.73; H, 5.59; Cl, 11.56; N, 13.70; O, 10.43. Found: C, 58.87; H, 5.51; N, 13.52.

***3**·2HCl.* Yield = 19.4%; dark-violet solid; mp dec >200 °C. ^{1}H NMR (300 MHz, CD_3OD): 8.1 (s, 1H), 7.15 (dd, *J* = 3.4, 6.0 Hz, 2H), 7.03 (dd, *J* = 3.4, 6.0 Hz, 2H), 4.17 (m, 4H), 3.25 (m, 4H), 2.94 (s, 12H), 2.16 (m, 4H). ^{13}C NMR (75 MHz, CD_3OD): 166.5, 166.1, 163.9, 163.6, 152.4, 144.3, 132.5, 130.3, 129.0, 128.9, 128.3, 128.1, 126.6, 123.1, 121.1, 120.4, 118.4, 118.2, 97.0, 79.8, 57.1, 43.9, 38.7, 38.5, 24.9, 24.7. Anal. Calcd for $C_{30}H_{33}BrCl_2N_6O_4$: C, 52.04; H, 4.80; Br, 11.54; Cl, 10.24; N, 12.14; O, 9.24. Found: C, 52.17; H, 4.81; N, 12.12.

***4**·2HCl.* Yield = 11.2%; dark-violet solid; mp dec >200 °C. ^{1}H NMR (300 MHz, CD_3OD): 8.04 (s, 2H), 7.88 (d, *J* = 6.6 Hz, 1H), 7.84 (1H, s), 7.07 (d, *J* = 6.5 Hz, 1H), 4.2 (bs, 4H), 3.27 (m, 4H), 2.94 (s, 12H), 2.17 (m, 4H). ^{13}C NMR (75 MHz, CD_3OD):166.9, 166.7, 164.5, 134.6, 132.1, 129.6, 127.3, 127.2, 126.9, 126.6, 124.3, 124.1, 122.8, 117.8, 112.9, 99.6, 99.4, 57.0, 43.8, 38.4, 24.8. Anal. Calcd for $C_{30}H_{33}Cl_2N_7O_6$: C, 54.72; H, 5.05; Cl, 10.77; N, 14.89; O, 14.58. Found: C, 54.80; H, 5.01; N, 14.92.

***5**·2HCl.* Yield = 18.9%; dark-violet solid; mp dec >200 °C. ^{1}H NMR (300 MHz, CD_3OD): 8.00 (s, 1H), 7.87 (d, *J* = 6.6 Hz, 1H), 7.79 (1H, s), 7.0 (d, *J* = 6.5 Hz, 1H), 3.98 (bs, 4H), 3.14 (m, 4H), 2.83 (s, 12H), 2.01 (m, 4H). ^{13}C NMR (75 MHz, CD_3OD):162.0, 161.0, 144.6, 141.4, 140.7, 132.1, 127.1, 124.1, 122.9, 122.1, 121.2, 120.7, 118.9, 111.9, 55.1, 48.7, 46.5, 42.6, 37.5, 37.2, 22.5, 22.4. Anal. Calcd for $C_{30}H_{32}BrCl_2N_7O_6$: C, 48.86; H, 4.37; Br, 10.84; Cl, 9.61; N, 13.30; O, 13.02. Found: C, 48.79; H, 4.31; N, 13.22.

***8**·2HCl.* Yield = 18%; dark-violet solid; mp dec >200 °C. ^{1}H NMR (400 MHz, CD_3OD): 7.85 (s, 1H), 7.76 (s, 1H), 7.20 (m, 1H), 6.95 (bs, 1H), 3.91 (m, 4H), 2.70 (m, 4H), 2.52 (m, 12H), 1.93 (m, 4H). ^{13}C NMR (100 MHz, CD_3OD):165.8, 162.5, 161.5, 146.5, 143.8, 141.9, 133.2, 128.7, 125.5, 125.1, 123.4, 123.1, 121.9, 120.5, 97.8, 57.9, 45.2, 45.1, 39.9, 39.7, 26.0, 25.9. Anal. Calcd for $C_{29}H_{32}BrCl_2N_7O_4$: C, 50.23; H, 4.65; Br, 11.52; Cl, 10.22; N, 14.14; O, 9.23. Found: C, 50.17; H, 4.71; N, 14.08.

*Synthesis of **6** and **7**.* NDI **1** (0.5 mmol) was dissolved into 40 mL of CH_3CN in a round-bottom flask together with 1.0 mmol of 3,4-

DOI: 10.1021/acs.jmedchem.5b01283
J. Med. Chem. 2015, 58, 9639−9652

diaminobenzoic acid, the mixture was stirred at 85 °C for 72 h under argon. The resulting dark-violet solution was cooled at r.t. to induce precipitation of the product. The crude powder was filtered and purified by HPLC chromatography, (CH_3CN:H_2O 0.1%TFA) according to analytical method A and preparative method B, affording the title NDIs **6** (27%) and **7** (30.5%).

***6**·2HCl*. Yield = 27%; dark-violet solid; mp dec >200 °C. ^{1}H NMR (400 MHz, CD_3OD): 7.86 (s, 2H), 7.62 (d, J = 8.0 Hz, 1H), 7.39 (s, 1H), 6.89 (d, J = 8.0 Hz, 1H), 4.16 (m, 4H), 3.26 (m, 4H), 2.95 (s, 12H), 2.16 (m, 4H). ^{13}C NMR (100 MHz, CD_3OD):168.2, 166.6, 166.5, 164.3, 164.2, 143.1, 142.8, 132.6, 129.8, 129.2, 128.6, 127.0, 126.7, 126.6, 126.4, 123.6, 123.5, 119.0, 117.7, 98.3, 97.7, 57.0, 43.8, 40.7, 38.4; 24.8. Anal. Calcd for $C_{31}H_{34}Cl_2N_6O_6$: C, 56.63; H, 5.21; Cl, 10.78; N, 12.78; O, 14.60. Found: C, 56.77; H, 5.31; N, 12.72.

***7**·2HCl*. Yield = 30.5%; dark-violet solid; mp dec >200 °C. ^{1}H NMR (300 MHz, CD_3OD): 8.37 (s, 2H), 7.85 (d, J = 8.0 Hz, 1H), 7.73 (s, 1H), 7.21 (d, J = 8.0 Hz, 1H), 4.35 (m, 4H), 3.41 (m, 4H), 3.05 (s, 12H), 2.29 (m, 4H). ^{13}C NMR (75 MHz, CD_3OD): 168.3, 166.2, 163.5, 161.8, 161.7, 160.8, 152.2, 133.2, 132.6, 130.1, 129.4, 126.5, 123.4, 123.3, 121.6, 119.12, 118.21, 117.9, 98.3, 97.6, 57.04, 43.9, 38.3, 38.5, 24.8, 24.7. Anal. Calcd for $C_{31}H_{33}BrCl_2N_6O_6$: C, 50.56; H, 4.52; N, 11.41; O, 13.03. Found: C, 50.34; H, 4.61; N, 11.29

*Microwave Assisted (MW) Nucleophilic Aromatic Substitution: Synthesis of **9***. Compound **3** (0.5 mmol) was dissolved into 4 mL of *N*,*N*-dimethyl-propan-1,3-diamine. The mixture was stirred and heated in a microwave reactor, according to a closed vessel protocol, at 150 °C, 250 psi, 200 W, for 3 min. The resulting green solution was cooled at rt to induce precipitation of the product. The resulting deep-green powder was filtered and washed by water afforded **1** (Yield 92%). Further HPLC preparative purification (CH_3CN:H_2O and 0.1% CF_3COOH as eluent), and final trifluoroacetate-chloride anion exchange, by addition of 1 mL HCl 1M, yielded **9** as trihydrochloride (**9**·3HCl); deep-green solid; mp dec >200 °C. ^{1}H NMR (300 MHz, CD_3OD): δ = 7.10 (m, 1H), 6.96 (m, 2H), 6.69 (m, 2H), 4.11 (m, 4H), 3.42 (m, 2H), 3.26 (m, 6H), 2.99 (s, 6H), 2.93 (s, 12H), 2.18 (bs, 2H), 2.11 (bs, 4H). ^{13}C NMR (75 MHz, CD_3OD): δ = 166.7, 166.4, 164.5, 144.2, 139.7, 129.8, 129.0, 128.9, 127.5, 126.6, 125.0, 117.6, 117.1, 115.8, 108.2, 104.5, 98.1, 97.7, 63.4, 57.0, 54.0, 53.8, 43.8, 41.1, 38.5, 38.1, 25.7, 24.9, 24.8, 24.1. Anal. Calcd for $C_{35}H_{47}Cl_3N_8O_4$: C, 56.04; H, 6.32; Cl, 14.18; N, 14.94; O, 8.53. Found: C, 56.17; H, 6.39; N, 14.90.

*Exhaustive Methylation: Synthesis of **10** and **11***. The **c-exNDIs** (**2** or **3**) purified as hydrochlorides were dissolved in a $NaHCO_3$ solution and extracted 3 times with CH_2Cl_2. The recovered organic layers have been dried on Na_2SO_4 and the solvent evaporated under reduced pressure. The collected amine (2.5 mmol) was suspended in 50 mL of $CHCl_3$ and 1.2 g (8.5 mmol) of CH_3I were added. This suspension was stirred under nitrogen atmosphere, at room temperature for 12 h. After this period the resulting dark-violet powder was filtered and dried, afforded the product as pure di-iodide salt.

10. Yield = 99%; dark-violet crystals; mp dec >200 °C. ^{1}H NMR (400 MHz, CD_3OD): δ = 7.94 (s, 2H), 7.12 (dd, J = 3.3, 6.0 Hz, 2H), 6.97 (dd, J = 3.3, 6.0 Hz, 2H), 4.14 (m, 4H), 3.49 (m, 4H), 3.15 (m, 18H), 2.21 (m, 4H). ^{13}C NMR (100 MHz, D_2O): δ = 166.9, 165.8, 143.8, 129.1, 128.1, 127.6, 126.3, 123.5, 118.3, 97.5, 66.1, 54.1, 38.6, 23.6. Anal. Calcd for $C_{32}H_{38}I_2N_6O_4$: C, 46.62; H, 4.65; I, 30.78; N, 10.19; O, 7.76. Found: C, 46.53; H, 4.59; N, 10.22.

11. Yield = 99%; dark-violet crystals; mp dec >200 °C. ^{1}H NMR (400 MHz, CD_3OD): δ = 8.04 (s, 1H), 7.15 (bs, 2H), 7.00 (bs, 2H), 4.12 (m, 4H), 3.51 (m, 4H), 3.15 (s, 18H), 2.20 (bs, 2H). ^{13}C NMR (100 MHz, CD_3OD): δ = 166.3, 165.9, 163.2, 162.2, 145.1, 144.1, 143.0, 132.5, 130.1, 128.8, 128.7, 128.3, 128.2, 126.4, 123.0, 121.1, 120.2, 118.3, 118.2, 96.9, 65.8, 53.9, 38.8, 38.6, 23.3, 23.2. Anal. Calcd for $C_{32}H_{37}BrI_2N_6O_4$: C, 42.55; H, 4.13; Br, 8.84; I, 28.09; N, 9.30; O, 7.08. Found: C, 42.60; H, 4.18; N, 9.39.

Spectroscopic Techniques (FRET and CD). All oligonucleotides used in this study were from Sigma-Aldrich (Milan, Italy). For fluorescence melting curves, equimolar amounts of the compounds were added to each FAM (6-carboxyfluorescein) 5′-end- and TAMRA (6-carboxy-tetramethylrhodamine) 3′-end-labeled oligonucleotide (0.25 uM) folded in the lithium cacodylate buffer supplemented with potassium (100 mM). After stabilization at 4 °C, samples were processed in a LightCycler II (Roche, Milan, Italy) or LightCycler 480 (Roche, Milan, Italy), and the oligonucleotide melting was monitored by observing 6-carboxyfluorescein (6-FAM) emission in the temperature range of 30− 95 °C with 1 °C/min gradient. Melting profiles were normalized as previously described.[66] T_m was defined as the temperature corresponding to the 0.5 fraction of the normalized fluorescence.

For CD analysis, oligonucleotides were diluted to a final concentration of 4 μM in lithium cacodylate buffer (10 mM, pH 7.4) and KCl 100 mM. After annealing step (95 °C for 5 min), DNA samples were gradually cooled to room temperature and compounds added from stock at final concentration of 16 μM. CD spectra were recorded on a Chirascan-Plus (Applied Photophysisics, Leatherhead, UK) equipped with a Peltier temperature controller using a quartz cell of 5 mm optical path length and an instrument scanning speed of 50 nm/min over a wavelength range of 230−320 nm. The reported spectrum of each sample represents the average of 2 scans is baseline-corrected for signal contributions due to the buffer. Observed ellipticities were converted to mean residue ellipticity (θ) = deg × cm^2 × $dmol^{-1}$ (mol ellip). For the determination of T_m, spectra were recorded over a temperature range of 20−95 °C, with temperature increase of 5 °C/min. T_m values were calculated according to the van't Hoff equation, applied for a two-state transition from a folded to unfolded state, assuming that the heat capacity of the folded and unfolded states are equal.[67]

***Taq* Polymerase Stop Assay.** *Taq* polymerase stop assay was carried out as previously described.[27,30] Briefly, the 5′-end labeled primer was annealed to its template (Supporting Information, Table S1) in lithium cacodylate buffer in the presence or absence of KCl 100 mM and by heating at 95 °C for 5 min and gradually cooling to room temperature. Where specified, samples were incubated with **2** (3.1−25.0 nM). Primer extension was conducted with 2 U of AmpliTaq Gold DNA polymerase (Applied Biosystem, Carlsbad, California, USA) at 47 °C for 30 min. Reactions were stopped by ethanol precipitation, primer extension products were separated on a 15% denaturing gel, and finally visualized by phosphorimaging (Typhoon FLA 9000).

Mass Spectrometric (MS) Competition Assay. Oligonucleotides were heat-denatured and folded in 10 mM KCl, 150 mM trimethylammonium acetate (TMAA), pH 6.8, overnight at room temperature. The oligonucleotides where diluted to final concentration of 10 μM and incubated with the tested compound at ratio DNA:compound 1:1 overnight at 4 °C.

Samples were analyzed by direct infusion electrospray ionization (ESI) on a Xevo G2-XS QTof mass spectrometer (Waters, Manchester, UK). The injection was automatically performed by an Agilent 1290 Infinity HPLC (Agilent Technologies, Santa Clara, CA, US) equipped with an auto sampler; the carrying buffer was TMAA 100 mM. The absence of potassium in the carrying buffer allows the dilution of the salts before MS analysis decreasing the signal suppression. Up to 5 μL samples were typically injected for each analysis. The electrospray capillary was at 1.8 kV, the source and desolvation temperatures were 45 and 65 °C, respectively, and the sampling cone was at 65 V. All these parameters ensured minimal fragmentation of the DNAs complexes. The instrument was calibrated using a 2 mg/mL solution of sodium iodide in 50% 2-propanol. Additionally, the use of the LockSpray during the analysis provided a typical <2 ppm mass accuracy. The internal standard LockSpray consisted in a solution of leu-enkephalin 1 μg/mL in acetonitrile/water (50:50, v/v) containing 0.1% formic acid. Binding affinities were calculated for each experiment using the reconstructed-ion chromatogram area for each species calculated by MassLynx V4.1: this analysis was made possible by the experimental design that used an HPLC system to inject the samples in the mass spectrometer. The binding affinity was calculated with the following formula: [BA = ($\Sigma G4_b$/($\Sigma G4_f$ + $\Sigma G4_b$)) × 100], where BA is the binding affinity, $G4_b$ is chromatogram area of bound G4 DNA, and $G4_f$ is the chromatogram area of free G4 DNA.[68] $G4_b$ comprises DNA with one or two bound

DOI: 10.1021/acs.jmedchem.5b01283
J. Med. Chem. 2015, 58, 9639−9652

ligands, where present. Signals with charge states 6^-, 5^-, and 4^- were used for the free and bound hTel DNA and c-myc, charge states 6^- and 5^- for LTR-III, charge states 5^- and 4^- for c-kit2, and charge state 4^- for LTR-IV. Free DNA mono and dipotassium adducts were included in the calculation. For stoichiometric calculation, oligonucleotides were folded in 10 mM KCl, 150 mM TMAA pH 6.8 overnight at rt. The oligonucleotides, diluted to final concentration of 10 μM, were incubated with the tested compound (ratio 1:5, 1:10, 1:20, and 1:50) at 4 °C and analyzed by ESI-MS.

SPR Analysis. SPR was performed on the Biacore T100 platform (GE Healthcare). 5′-Biotinylated LTR-III, LTR-IV, and hTel oligonucleotides were heated at 95 °C for 5 min and cooled down at room temperature to allow G4 folding. Immobilization was performed in HEPES-KCl running buffer (0.01 M HEPES pH 7.4, 0.2 M KCl, 3 mM EDTA) on a steptavidin coated surface (SA sensor chip, Biacore). Oligonucleotides were diluted in HEPES-KCl running buffer to a concentration of 30 nM and injected to reach the response of around 500 RU. Flow cell 1 was left empty to allow reference subtraction. **C-exNDIs** binding analysis was performed at a flow rate of 30 μL/min, with contact time of 280 s and dissociation time of 360 s in HEPES-KCl buffer. Sensorgrams were obtained in the concentration range of 25−200 nM. After each compound injection the chip surface was regenerated with glycine 10 mM pH 2.0 solution (GE Healthcare). All sensorgrams were corrected by buffer injection response. Data were fitted to a 1:1 binding model with R_{max} initial parameter set to theoretical calculated R_{max} using BIAevaluation software (GE Healthcare). All experiments were performed independently at least twice, and in each instance χ^2 values, which indicate the goodness of fitting, were below 0.2.

CL-Mediated Footprinting. All oligonucleotides were gel-purified before use and prepared in desalted/lyophilized form. Oligonucleotides were 5′-end-labeled with [γ-^{32}P]ATP by T4 polynucleotide kinase and purified by MicroSpin G-25 columns (GE Healthcare, Europe). They were next resuspended in lithium cacodylate 10 mM, pH 7.4, and KCl 100 mM, heat-denatured, and folded. Reactions of the labeled G-quadruplex folded oligonucleotides (4 pmol/sample) with increasing amounts of compound **2** (4−100 nM) were performed at 20 °C for 24 h in resuspension buffer. Samples were then reacted with CL (100 μM) at 37 °C for 24 h. Reactions were stopped by ethanol precipitation, resuspended, and either kept on ice or treated at 90 °C for 30 min with 1 M piperidine to complete strand scission according to the Maxam and Gilbert protocol. Samples were then lyophilized, resuspended in formamide gel loading buffer, and heated at 95 °C for 3 min. Reaction products were analyzed on 20% denaturing polyacrylamide gels and visualized by Typhoon FLA 9000 phosphorimaging analysis (GE Healthcare).

Reporter Assays. The HIV-1 promoter activity in live cells in the presence of **2** was monitored in HeLa-Tat-III/LTR/d1EGFP cells (obtained through the NIH AIDS Reagent Program, Division of AIDS, NIAID, NIH, from Dr. Satoh). This cell line derives from HeLa-tat-III and is transfected with d1EGFP under the control of HIV-1 LTR promoter. Then 8 $\times 10^4$ of HeLa-Tat-III/LTR/d1EGFP cells were seeded in a 12-well plate in 1 mL of DMEM/10% FBS medium supplemented with Geneticin selective antibiotic (1 mg/mL, Life Technologies, Monza, Italy) and incubated overnight. Cells were next treated with increasing concentrations of **2** (0−62.5−125−250 nM) and incubated at 37 °C. After 48 h, cells were washed with PBS 1× and resuspended in 500 μL of PBS 1×. To evaluate the mean of EGFP fluorescence, a total of 10000 events were acquired for each sample with an LRS 2 instrument using FACS DIVA Software (BD Bioscience) and analyzed with Flow Jo (Tree Star). Cell debris and dead cells were excluded from the analysis by gating on forward scatter (FSC) versus side scatter (SSC) and were quantified to estimate the cytotoxicity.

For the luciferase assay, HIV-1 LTR region (wt or M4 + 5) was inserted into the promoterless luciferase reporter vector pGL4.10-Luc2 (Promega Italia, Italy), as previously reported.[27] For assessment of luciferase activity, human embryonic kidney 293T (HEK293T) cells were seeded in a 24-well plate (9 × 10^4 cells/well). Then 24 h later, cells were transfected with 100 ng/well of pGL4.10-LTRwt or of pGL4.10-LTR-M4 + 5 using TransIT-293 transfection reagent (Mirus Bio LLC, Madison, WI, USA), according to the manufacturer's protocol. After 1 h, cells were treated with **2** for 24 h at various concentrations. Luciferase activity was measured using the britelite plus Reporter Gene Assay System (PerkinElmer Inc., Milan, Italy) at a Victor X2 multilabel plate reader (PerkinElmer Inc., Milan, Italy), according to the manufacturer's instructions. Cells were lysed in RIPA buffer (50 mM Tris-HCl pH 7.2, 150 mM NaCl, 1% Igepal, 0.1% SDS) and protein concentration was determined by BCA assay (Thermo Scientific Pierce, Monza, Italy). Luciferase signals were subsequently normalized to total protein content, according to the manufacturer's protocol (http://ita.promega.com/~/pdf/resources/pubhub/cellnotes/normalizing-genetic-reporter-assays/).

Antiviral Assay in HIV-1 Infected TZM-bl Cells. HIV-1 infectivity was measured using the TZM-bl reporter cell line (obtained through the NIH AIDS Reagent Program, Division of AIDS, NIAID, NIH, from Dr. J.C. Kappes, Dr. X. Wu, and Tranzyme Inc.). TZM-bl is a HeLa cell line stably expressing large amounts of CD4 and CCR5 and containing integrated copies of the luciferase and β-galactosidase genes under control of the HIV-1 promoter. TZM-bl were grown in DMEM supplemented with 10% FBS. Cells (1 $\times 10^4$ cells/well) were seeded in 96-well plates and grown overnight to permit adherence prior to treatment and viral infection. Cells were next infected with HIV-1 NL4-3 strain or BaL strain at a MOI of 0.5, treated with serial dilutions of tested compounds, and incubated at 37 °C. After 48 h, cells were washed with PBS 1× and HIV-1 production was assessed following the LTR-luciferase signal using the britelite plus Reporter Gene Assay System (PerkinElmer, Waltman, MA, USA) according to the manufacturer's protocol.

Cytotoxicity Assay. Cytotoxicity of tested compounds was tested in parallel to antiviral and reporter assays by MTT. The 50% cytotoxic concentration (CC_{50}) was defined as the concentration of test compound that was able to reduce the absorbance of the mock-infected cells by 50%. The 50% inhibitory concentration (IC_{50}) was defined as the concentration of test compound that inhibit 50% of LTR-Luciferase signal. The selectivity index (SI) is the relative effectiveness of the tested compound in inhibiting viral replication compared to inducing cell death (CC_{50} value/IC_{50} value). The therapeutic window (TW) is the concentration range at which the compound shows antiviral activity paralleled by less than 80% cytotoxicity.

HIV-1 Entry Assay. TZM-bl cells (1 × 10^4 cells/well) were seeded in 96-well plates and grown overnight to permit adherence prior to treatment and viral infection. Cells were next infected with HIV-1 NL4-3 (MOI 0.5) and incubated at 37 °C. Compound **2** (50−100 nM) and the reference compounds DS (100 μg/mL, Sigma-Aldrich) and AZT (0.5 μg/mL, Sigma-Aldrich) were added at different hours (0, 1, 2 h) pi. After 31 h, cells were washed with PBS 1× and HIV-1 production was assessed following the LTR-luciferase signal using the britelite plus Reporter Gene Assay System (PerkinElmer, Waltman, MA, USA) according to the manufacturer's protocol.

Computational Method. DFT calculations were performed with the Gaussian 09, revision B.01 software package.[69] Gas-phase geometry optimizations were carried out using the B3LYP functional,[70] with 6-31+G(d,p) basis set for all the atoms.

■ ASSOCIATED CONTENT

Supporting Information

The Supporting Information is available free of charge on the ACS Publications website at DOI: 10.1021/acs.jmedchem.5b01283.

Additional figures illustrating all oligonucleotides used in this study, CD spectra, and the complete ESI/MS competition analysis (PDF)

Molecular formula strings (CSV)

DOI: 10.1021/acs.jmedchem.5b01283
J. Med. Chem. 2015, 58, 9639−9652

AUTHOR INFORMATION

Corresponding Authors

*For M.F.: phone, +39 0382 987668; fax, +39 0382 987323; E-mail, mauro.freccero@unipv.it.

*For S.N.R.: phone, +39 049 8272346; fax, +39 049 8272355; E-mail, sara.richter@unipd.it.

Author Contributions

§R.P., F.D., and E.B. contributed equally.

Notes

The authors declare no competing financial interest.

ACKNOWLEDGMENTS

This work was supported by the Bill and Melinda Gates Foundation (GCE grant numbers OPP1035881, OPP1097238) to S.N.R., the European Research Council (ERC Consolidator grant 615879) to S.N.R. and M.F., and the Italian Ministry of University and Research (FIRB-Ideas RBID082ATK) to S.N.R. and M.F. We thank Prof. Manlio Palumbo, University of Padua, for helpful comments on the manuscript.

ABBREVIATIONS USED

G4, G-quadruplex; NDI, naphthalene diimide; c-exNDI, core-extended NDI; LTR, long terminal repeat; ds, double-stranded; T_m, melting temperature

REFERENCES

(1) Lipps, H. J.; Rhodes, D. G-quadruplex structures: in vivo evidence and function. *Trends Cell Biol.* **2009**, *19*, 414−422.

(2) Sen, D.; Gilbert, W. Formation of parallel four-stranded complexes by guanine-rich motifs in DNA and its implications for meiosis. *Nature* **1988**, *334*, 364−366.

(3) Wu, Y.; Brosh, R. M., Jr. G-quadruplex nucleic acids and human disease. *FEBS J.* **2010**, *277*, 3470−3488.

(4) Sen, D.; Gilbert, W. A sodium-potassium switch in the formation of four-stranded G4-DNA. *Nature* **1990**, *344*, 410−414.

(5) Taylor, J. P. Neurodegenerative diseases: G-quadruplex poses quadruple threat. *Nature* **2014**, *507*, 175−177.

(6) Campbell, N. H.; Neidle, S. G-quadruplexes and metal ions. *Met. Ions Life Sci.* **2012**, *10*, 119−134.

(7) Eddy, J.; Maizels, N. Gene function correlates with potential for G4 DNA formation in the human genome. *Nucleic Acids Res.* **2006**, *34*, 3887−3896.

(8) Huppert, J. L.; Balasubramanian, S. G-quadruplexes in promoters throughout the human genome. *Nucleic Acids Res.* **2007**, *35*, 406−413.

(9) Nakken, S.; Rognes, T.; Hovig, E. The disruptive positions in human G-quadruplex motifs are less polymorphic and more conserved than their neutral counterparts. *Nucleic Acids Res.* **2009**, *37*, 5749−5756.

(10) Cogoi, S.; Xodo, L. E. G-quadruplex formation within the promoter of the KRAS proto-oncogene and its effect on transcription. *Nucleic Acids Res.* **2006**, *34*, 2536−2549.

(11) Eddy, J.; Maizels, N. Conserved elements with potential to form polymorphic G-quadruplex structures in the first intron of human genes. *Nucleic Acids Res.* **2008**, *36*, 1321−1333.

(12) Verma, A.; Yadav, V. K.; Basundra, R.; Kumar, A.; Chowdhury, S. Evidence of genome-wide G4 DNA-mediated gene expression in human cancer cells. *Nucleic Acids Res.* **2009**, *37*, 4194−4204.

(13) Mani, P.; Yadav, V. K.; Das, S. K.; Chowdhury, S. Genome-wide analyses of recombination prone regions predict role of DNA structural motif in recombination. *PLoS One* **2009**, *4*, e4399.

(14) Haeusler, A. R.; Donnelly, C. J.; Periz, G.; Simko, E. A.; Shaw, P. G.; Kim, M. S.; Maragakis, N. J.; Troncoso, J. C.; Pandey, A.; Sattler, R.; Rothstein, J. D.; Wang, J. C9orf72 nucleotide repeat structures initiate molecular cascades of disease. *Nature* **2014**, *507*, 195−200.

(15) Ivanov, P.; O'Day, E.; Emara, M. M.; Wagner, G.; Lieberman, J.; Anderson, P. G-quadruplex structures contribute to the neuroprotective effects of angiogenin-induced tRNA fragments. *Proc. Natl. Acad. Sci. U. S. A.* **2014**, *111*, 18201−18206.

(16) Sket, P.; Pohleven, J.; Kovanda, A.; Stalekar, M.; Zupunski, V.; Zalar, M.; Plavec, J.; Rogelj, B. Characterization of DNA G-quadruplex species forming from C9ORF72 G4C2-expanded repeats associated with amyotrophic lateral sclerosis and frontotemporal lobar degeneration. *Neurobiol. Aging* **2015**, *36*, 1091−1096.

(17) Fisette, J. F.; Montagna, D. R.; Mihailescu, M. R.; Wolfe, M. S. A G-rich element forms a G-quadruplex and regulates BACE1 mRNA alternative splicing. *J. Neurochem.* **2012**, *121*, 763−773.

(18) Fry, M.; Loeb, L. A. The fragile X syndrome d(CGG)n nucleotide repeats form a stable tetrahelical structure. *Proc. Natl. Acad. Sci. U. S. A.* **1994**, *91*, 4950−4954.

(19) Sissi, C.; Gatto, B.; Palumbo, M. The evolving world of protein-G-quadruplex recognition: a medicinal chemist's perspective. *Biochimie* **2011**, *93*, 1219−1230.

(20) Biffi, G.; Tannahill, D.; McCafferty, J.; Balasubramanian, S. Quantitative visualization of DNA G-quadruplex structures in human cells. *Nat. Chem.* **2013**, *5*, 182−186.

(21) Henderson, A.; Wu, Y.; Huang, Y. C.; Chavez, E. A.; Platt, J.; Johnson, F. B.; Brosh, R. M., Jr.; Sen, D.; Lansdorp, P. M. Detection of G-quadruplex DNA in mammalian cells. *Nucleic Acids Res.* **2014**, *42*, 860−869.

(22) Metifiot, M.; Amrane, S.; Litvak, S.; Andreola, M. L. G-quadruplexes in viruses: function and potential therapeutic applications. *Nucleic Acids Res.* **2014**, *42*, 12352−12366.

(23) Murat, P.; Zhong, J.; Lekieffre, L.; Cowieson, N. P.; Clancy, J. L.; Preiss, T.; Balasubramanian, S.; Khanna, R.; Tellam, J. G-quadruplexes regulate Epstein-Barr virus-encoded nuclear antigen 1 mRNA translation. *Nat. Chem. Biol.* **2014**, *10*, 358−364.

(24) Norseen, J.; Johnson, F. B.; Lieberman, P. M. Role for G-quadruplex RNA binding by Epstein-Barr virus nuclear antigen 1 in DNA replication and metaphase chromosome attachment. *J. Virol.* **2009**, *83*, 10336−10346.

(25) Tan, J.; Vonrhein, C.; Smart, O. S.; Bricogne, G.; Bollati, M.; Kusov, Y.; Hansen, G.; Mesters, J. R.; Schmidt, C. L.; Hilgenfeld, R. The SARS-unique domain (SUD) of SARS coronavirus contains two macrodomains that bind G-quadruplexes. *PLoS Pathog.* **2009**, *5*, e1000428.

(26) Perrone, R.; Nadai, M.; Poe, J. A.; Frasson, I.; Palumbo, M.; Palu, G.; Smithgall, T. E.; Richter, S. N. Formation of a unique cluster of G-quadruplex structures in the HIV-1 Nef coding region: implications for antiviral activity. *PLoS One* **2013**, *8*, e73121.

(27) Perrone, R.; Nadai, M.; Frasson, I.; Poe, J. A.; Butovskaya, E.; Smithgall, T. E.; Palumbo, M.; Palu, G.; Richter, S. N. A dynamic G-quadruplex region regulates the HIV-1 long terminal repeat promoter. *J. Med. Chem.* **2013**, *56*, 6521−6530.

(28) Amrane, S.; Kerkour, A.; Bedrat, A.; Vialet, B.; Andreola, M. L.; Mergny, J. L. Topology of a DNA G-quadruplex structure formed in the HIV-1 promoter: a potential target for anti-HIV drug development. *J. Am. Chem. Soc.* **2014**, *136*, 5249−5252.

(29) Piekna-Przybylska, D.; Sullivan, M. A.; Sharma, G.; Bambara, R. A. U3 region in the HIV-1 genome adopts a G-quadruplex structure in its RNA and DNA sequence. *Biochemistry* **2014**, *53*, 2581−2593.

(30) Perrone, R.; Butovskaya, E.; Daelemans, D.; Palu, G.; Pannecouque, C.; Richter, S. N. Anti-HIV-1 activity of the G-quadruplex ligand BRACO-19. *J. Antimicrob. Chemother.* **2014**, *69*, 3248−3258.

(31) Cogoi, S.; Paramasivam, M.; Spolaore, B.; Xodo, L. E. Structural polymorphism within a regulatory element of the human KRAS promoter: formation of G4-DNA recognized by nuclear proteins. *Nucleic Acids Res.* **2008**, *36*, 3765−3780.

(32) Siddiqui-Jain, A.; Grand, C. L.; Bearss, D. J.; Hurley, L. H. Direct evidence for a G-quadruplex in a promoter region and its targeting with a small molecule to repress c-MYC transcription. *Proc. Natl. Acad. Sci. U. S. A.* **2002**, *99*, 11593−11598.

DOI: 10.1021/acs.jmedchem.5b01283
J. Med. Chem. 2015, 58, 9639−9652

(33) Campbell, N. H.; Parkinson, G. N.; Reszka, A. P.; Neidle, S. Structural basis of DNA quadruplex recognition by an acridine drug. *J. Am. Chem. Soc.* **2008**, *130*, 6722−6724.
(34) Leonetti, C.; Amodei, S.; D'Angelo, C.; Rizzo, A.; Benassi, B.; Antonelli, A.; Elli, R.; Stevens, M. F.; D'Incalci, M.; Zupi, G.; Biroccio, A. Biological activity of the G-quadruplex ligand RHPS4 (3,11-difluoro-6,8,13-trimethyl-8H-quino[4,3,2-kl]acridinium methosulfate) is associated with telomere capping alteration. *Mol. Pharmacol.* **2004**, *66*, 1138−1146.
(35) Balasubramanian, S.; Hurley, L. H.; Neidle, S. Targeting G-quadruplexes in gene promoters: a novel anticancer strategy? *Nat. Rev. Drug Discovery* **2011**, *10*, 261−275.
(36) Ali, A.; Bhattacharya, S. DNA binders in clinical trials and chemotherapy. *Bioorg. Med. Chem.* **2014**, *22*, 4506−4521.
(37) Franceschin, M.; Rossetti, L.; D'Ambrosio, A.; Schirripa, S.; Bianco, A.; Ortaggi, G.; Savino, M.; Schultes, C.; Neidle, S. Natural and synthetic G-quadruplex interactive berberine derivatives. *Bioorg. Med. Chem. Lett.* **2006**, *16*, 1707−1711.
(38) Kim, M. Y.; Vankayalapati, H.; Shin-Ya, K.; Wierzba, K.; Hurley, L. H. Telomestatin, a potent telomerase inhibitor that interacts quite specifically with the human telomeric intramolecular g-quadruplex. *J. Am. Chem. Soc.* **2002**, *124*, 2098−2099.
(39) Dai, J.; Carver, M.; Hurley, L. H.; Yang, D. Solution structure of a 2:1 quindoline-c-MYC G-quadruplex: insights into G-quadruplex-interactive small molecule drug design. *J. Am. Chem. Soc.* **2011**, *133*, 17673−17680.
(40) Fedoroff, O. Y.; Salazar, M.; Han, H.; Chemeris, V. V.; Kerwin, S. M.; Hurley, L. H. NMR-Based model of a telomerase-inhibiting compound bound to G-quadruplex DNA. *Biochemistry* **1998**, *37*, 12367−12374.
(41) Di Antonio, M.; Doria, F.; Richter, S. N.; Bertipaglia, C.; Mella, M.; Sissi, C.; Palumbo, M.; Freccero, M. Quinone methides tethered to naphthalene diimides as selective G-quadruplex alkylating agents. *J. Am. Chem. Soc.* **2009**, *131*, 13132−13141.
(42) Collie, G. W.; Promontorio, R.; Hampel, S. M.; Micco, M.; Neidle, S.; Parkinson, G. N. Structural basis for telomeric G-quadruplex targeting by naphthalene diimide ligands. *J. Am. Chem. Soc.* **2012**, *134*, 2723−2731.
(43) Micco, M.; Collie, G. W.; Dale, A. G.; Ohnmacht, S. A.; Pazitna, I.; Gunaratnam, M.; Reszka, A. P.; Neidle, S. Structure-based design and evaluation of naphthalene diimide G-quadruplex ligands as telomere targeting agents in pancreatic cancer cells. *J. Med. Chem.* **2013**, *56*, 2959−2974.
(44) Doria, F.; Nadai, M.; Sattin, G.; Pasotti, L.; Richter, S. N.; Freccero, M. Water soluble extended naphthalene diimides as pH fluorescent sensors and G-quadruplex ligands. *Org. Biomol. Chem.* **2012**, *10*, 3830−3840.
(45) Doria, F.; Oppi, A.; Manoli, F.; Botti, S.; Kandoth, N.; Grande, V.; Manet, I.; Freccero, M. A naphthalene diimide dyad for fluorescence switch-on detection of G-quadruplexes. *Chem. Commun. (Cambridge, U. K.)* **2015**, *51*, 9105−9108.
(46) Nadai, M.; Doria, F.; Germani, L.; Richter, S. N.; Freccero, M. A photoreactive G-quadruplex ligand triggered by green light. *Chem. - Eur. J.* **2015**, *21*, 2330−2334.
(47) Artusi, S.; Nadai, M.; Perrone, R.; Biasolo, M. A.; Palu, G.; Flamand, L.; Calistri, A.; Richter, S. N. The Herpes Simplex Virus-1 genome contains multiple clusters of repeated G-quadruplex: Implications for the antiviral activity of a G-quadruplex ligand. *Antiviral Res.* **2015**, *118*, 123−131.
(48) Doria, F.; di Antonio, M.; Benotti, M.; Verga, D.; Freccero, M. Substituted heterocyclic naphthalene diimides with unexpected acidity. Synthesis, properties, and reactivity. *J. Org. Chem.* **2009**, *74*, 8616−8625.
(49) Zhou, C.; Li, Y.; Zhao, Y.; Zhang, J.; Yang, W.; Li, Y. An unusual addition reaction for constructing a novel pH-controlled fluorescence switch. *Org. Lett.* **2011**, *13*, 292−295.
(50) Suraru, S. L.; Zschieschang, U.; Klauk, H.; Wurthner, F. A core-extended naphthalene diimide as a p-channel semiconductor. *Chem. Commun. (Cambridge, U. K.)* **2011**, *47*, 11504−11506.
(51) Langhals, H.; Kinzel, S. Laterally extended naphthalene tetracarboxylic bisimides. *J. Org. Chem.* **2010**, *75*, 7781−7784.
(52) Doria, F.; Manet, I.; Grande, V.; Monti, S.; Freccero, M. Water-soluble naphthalene diimides as singlet oxygen sensitizers. *J. Org. Chem.* **2013**, *78*, 8065−8073.
(53) Palm, W.; de Lange, T. How shelterin protects mammalian telomeres. *Annu. Rev. Genet.* **2008**, *42*, 301−334.
(54) Rosu, F.; Gabelica, V.; Houssier, C.; De Pauw, E. Determination of affinity, stoichiometry and sequence selectivity of minor groove binder complexes with double-stranded oligodeoxynucleotides by electrospray ionization mass spectrometry. *Nucleic Acids Res.* **2002**, *30*, e82.
(55) Yuan, G.; Zhang, Q.; Zhou, J.; Li, H. Mass spectrometry of G-quadruplex DNA: formation, recognition, property, conversion, and conformation. *Mass Spectrom. Rev.* **2011**, *30*, 1121−1142.
(56) Turner, K. B.; Hagan, N. A.; Fabris, D. Inhibitory effects of archetypical nucleic acid ligands on the interactions of HIV-1 nucleocapsid protein with elements of Psi-RNA. *Nucleic Acids Res.* **2006**, *34*, 1305−1316.
(57) Fernando, H.; Reszka, A. P.; Huppert, J.; Ladame, S.; Rankin, S.; Venkitaraman, A. R.; Neidle, S.; Balasubramanian, S. A conserved quadruplex motif located in a transcription activation site of the human c-kit oncogene. *Biochemistry* **2006**, *45*, 7854−7860.
(58) Nadai, M.; Palu, G.; Palumbo, M.; Richter, S. N. Differential targeting of unpaired bases within duplex DNA by the natural compound clerocidin: a valuable tool to dissect DNA secondary structure. *PLoS One* **2012**, *7*, e52994.
(59) Richter, S. N.; Menegazzo, I.; Nadai, M.; Moro, S.; Palumbo, M. Reactivity of clerocidin towards adenine: implications for base-modulated DNA damage. *Org. Biomol. Chem.* **2009**, *7*, 976−985.
(60) Nadai, M.; Sattin, G.; Palu, G.; Palumbo, M.; Richter, S. N. Clerocidin-mediated DNA footprinting discriminates among different G-quadruplex conformations and detects tetraplex folding in a duplex environment. *Biochim. Biophys. Acta, Gen. Subj.* **2013**, *1830*, 4660−4668.
(61) Doria, F.; Nadai, M.; Folini, M.; Di Antonio, M.; Germani, L.; Percivalle, C.; Sissi, C.; Zaffaroni, N.; Alcaro, S.; Artese, A.; Richter, S. N.; Freccero, M. Hybrid ligand-alkylating agents targeting telomeric G-quadruplex structures. *Org. Biomol. Chem.* **2012**, *10*, 2798−2806.
(62) Wilkinson, R. A.; Pincus, S. H.; Shepard, J. B.; Walton, S. K.; Bergin, E. P.; Labib, M.; Teintze, M. Novel compounds containing multiple guanide groups that bind the HIV coreceptor CXCR4. *Antimicrob. Agents Chemother.* **2011**, *55*, 255−263.
(63) Furman, P. A.; Fyfe, J. A.; St. Clair, M. H.; Weinhold, K.; Rideout, J. L.; Freeman, G. A.; Lehrman, S. N.; Bolognesi, D. P.; Broder, S.; Mitsuya, H. Phosphorylation of 3′-azido-3′-deoxythymidine and selective interaction of the 5′-triphosphate with human immunodeficiency virus reverse transcriptase. *Proc. Natl. Acad. Sci. U. S. A.* **1986**, *83*, 8333−8337.
(64) Mitsuya, H.; Looney, D. J.; Kuno, S.; Ueno, R.; Wong-Staal, F.; Broder, S. Dextran sulfate suppression of viruses in the HIV family: inhibition of virion binding to CD4+ cells. *Science* **1988**, *240*, 646−649.
(65) Czerwinska, I.; Juskowiak, B. Photoisomerizable arylstilbazolium ligands recognize parallel and antiparallel structures of G-quadruplexes. *Int. J. Biol. Macromol.* **2012**, *51*, 576−582.
(66) Rachwal, P. A.; Fox, K. R. Quadruplex melting. *Methods* **2007**, *43*, 291−301.
(67) Greenfield, N. J. Using circular dichroism collected as a function of temperature to determine the thermodynamics of protein unfolding and binding interactions. *Nat. Protoc.* **2007**, *1*, 2527−2535.
(68) Tan, W.; Zhou, J.; Yuan, G. Electrospray ionization mass spectrometry probing of binding affinity of berbamine, a flexible cyclic alkaloid from traditional Chinese medicine, with G-quadruplex DNA. *Rapid Commun. Mass Spectrom.* **2014**, *28*, 143−147.
(69) Frisch, M. J.; Trucks, G. W.; Schlegel, H. B.; Scuseria, G. E.; Robb, M. A.; Cheeseman, J. R.; Scalmani, G.; Barone, V.; Mennucci, B.; Petersson, G. A.; Nakatsuji, H.; Caricato, M.; Li, X.; Hratchian, H. P.; Izmaylov, A. F.; Bloino, J.; Zheng, G.; Sonnenberg, J. L.; Hada, M.;

DOI: 10.1021/acs.jmedchem.5b01283
J. Med. Chem. 2015, 58, 9639−9652

Ehara, M.; Toyota, K.; Fukuda, R.; Hasegawa, J.; Ishida, M.; Nakajima, T.; Honda, Y.; Kitao, O.; Nakai, H.; Vreven, T.; Montgomery, J. A., Jr., Peralta, J. E.; Ogliaro, F.; Bearpark, M.; Heyd, J. J.; Brothers, E.; Kudin, K. N.; Staroverov, V. N.; Keith, T.; Kobayashi, R.; Normand, J.; Raghavachari, K.; Rendell, A.; Burant, J. C.; Iyengar, S. S.; Tomasi, J.; Cossi, M.; Rega, N.; Millam, J. M.; Klene, M.; Knox, J. E.; Cross, J. B.; Bakken, V.; Adamo, C.; Jaramillo, J.; Gomperts, R.; Stratmann, R. E.; Yazyev, O.; Austin, A. J.; Cammi, R.; Pomelli, C.; Ochterski, J. W.; Martin, R. L.; Morokuma, K.; Zakrzewski, V. G.; Voth, G. A.; Salvador, P.; Dannenberg, J. J.; Dapprich, S.; Daniels, A. D.; Farkas, O.; Foresman, J. B.; Ortiz, J. V.; Cioslowski, J.; Fox, D. J. *Gaussian 09*, revision B.01; Gaussian, Inc.: Wallingford CT, 2010.

(70) Becke, A. D. Density-functional thermochemistry. III. The role of exact exchange. *J. Chem. Phys.* **1993**, *98*, 5648−5652.

DOI: 10.1021/acs.jmedchem.5b01283
J. Med. Chem. 2015, 58, 9639−9652